Roll Motion Response Analysis of Damaged Ships in Beam Waves

Lifen Hu [1], Hao Wu [2], Zhiming Yuan [3, 4], Wubin Li [1], Xiangyang Wang [1]

1. School of Transportation, Ludong University, Yantai 264025, China; 2. Sanjiang Astronautics Group, Yuanfang Technology Development Company, Wuhan, 430035, China; 3. Department of Naval Architecture, Ocean and Marine Engineering, University of Strathclyde, United Kingdom; 4. School of Naval Architecture and Ocean Engineering, Jiangsu University of Science and Technology

Abstract: The seakeeping performance of a damaged ship is highly correlated to the wave incident direction. Therefore, predicting the motion responses of a damaged ship under various incoming waves is important. In this study, the seakeeping performance of a DTMB 5415 model is investigated by focusing on its roll motion under beam wave condition. The model performance under an incident wave angle (α) of 180° is widely studied experimentally and numerically. But the behaviours of a damaged ship under α=0° remain unknown. This study aims to analyse the damaged ship motion performance under this rarely studied condition. The volume of fluid (VOF) free-surface technique is used to solve the Reynolds-averaged Navier–Stokes equations, as well as with the dynamic overset technology that handles the mesh update, the wave generation, time step and fast Fourier transform are utilised to validate the effectiveness of the adopted method. The numerical results are validated against the experimental results obtained when α=180°. The same methodology is extended to investigate the three-degrees-of-freedom motion (roll, pitch and heave) at α=0°. Results show that the roll motions under the two wave conditions greatly differ from each other. The discussions highlight the analysis of the possible reasons for this difference.

Key words: Beam wave; Motion response; Damaged ship; Roll motion

1. Introduction

The motion responses of damaged ship motion in waves are one of the primary concerns of marine safety. After a ship is damaged, the flooding water and wave excitation affect the ship's motion and vice versa. These complex interactions cause the ship motion in wave to exhibit strong nonlinearity and become a complex problem. Therefore, many studies were performed to investigate the damaged ship motion in wave.

The earliest investigation about the flooding motion in wave starts from potential flow theory, which analyses the ship and wave interaction through strip theory (Turan and Vassalos, 1993; Lee, 2007). A numerical method that coupled the ship motion with floodwater was presented to assess the stability of a damaged ferry in realistic environments, and the viscous effect was examined using the method proposed by Ikeda (Ikeda, 1978). By adopting a similar concept, de Kat and Pauling used the six-degrees-of-freedom (6-DOF) system to evaluate the extreme motions of a damaged ship in waves (de Kat and Pauling, 2001). The dynamic motion response of a damaged roll-on/roll-off (Ro-Ro) ship was also investigated (Chan et al., 2002). The findings of this investigation indicate that the nonlinear factor of the viscous effect should be comprehensively considered, especially in the context of dangerous waves. Studying floodwater motion through numerical simulations is

critical and challenging. On the basis of Bernoulli's equation and quasi-stationary assumption, a pressure correction technique was proposed to evaluate the ship motion (Ruponen, 2007). However, this method does not work well in drastic flooding cases. Therefore, this technique was improved by considering the water surface (Spanos and Papanikolaou, 2001; Manderbacka and Matusiak, 2011). According to the benchmark study of the International Towing Tank Conference (ITTC, 2002), the above-mentioned method cannot reliably predict the damage condition. Although the wave effect on the flooding process can be considered and the efficiency of the hydraulic model is high, effective and accurate methods are still required to investigate the damaged ship motion in waves (Ruponen, 2019).

With the rapid development of the computational capacity, the interest in applying computational fluid dynamic (CFD) simulations to evaluate the damaged ship motion increases. This approach mainly focuses on solving the Reynolds-averaged Navier–Stokes (RANS) equation with a free-surface capturing technique. The research on the damaged barge in calm water, which is the ITTC benchmark model for progressive flooding, was conducted (Straser, 2010; Gao, 2011; Hu, 2019), and the result of the simulation is consistent with that of the experiment. On the basis of this research, a numerical method that combines the RANS solver with the volume of fluid (VOF) model was developed to study the motion of a damaged Ro-Ro ferry ship in beam seas with waves from the same side of the damage (Gao, 2013; Bu, 2019). The roll response is consistent with the result obtained through experimental measurement. In addition, to analyse the coupled dynamics interaction between the damaged ship and the sea waves, in-house CFD codes CFDShip-Iowa (Sadat-Hosseini, 2006) and HUST-Ship (Wang, 2019) were combined with the 6-DOF ship motion model to solve the RANS equation. The heave, roll and pitch amplitudes of the damaged ship in beam waves were studied. Moreover, cases of sudden water flooding in the DTMB 5415 model in beam waves were investigated (Gao, 2020). Compared with the simplified model for flooding and damaged ship dynamics, the ability of the CFD method to address the flooding problem despite its strict requirements for calculation resource was confirmed in the above studies (Ruth, 2019). However, most present studies focus on the wave direction that comes from the same side of the damage, few researches highlight the behaviour of ship motion when the wave spreads from the opposite side of the damage, how the ship motion under this condition remain unknown, also this behaviour is an important aspect in ship safety and decision-making in case of emergency.

To analyse the relevant mechanism and identify the effect of two beam wave directions on the ship motion, namely, α=0° and α=180°, this study investigates the motion response characteristics of a DTMB 5415 model under waves that are incident from the opposite direction of the damaged side. Firstly, the validation of the wave generation, wave field and time step is conducted. Secondly, the simulation results of the

three-degrees-of-freedom (3-DOF) motion response (roll, pitch and heave motions) are presented, and the fast Fourier transform (FFT) algorithm is used to determine the maximal response frequency of the ship's roll motion. The roll response amplitude operators (RAOs) with different frequencies are examined in accordance with the validation of the damaged ship motion obtained through experiment (Begovic, 2013; Gu, 2019). Lastly, the ship motion analysis considering the regular beam waves from the opposite side is performed. The two wave directions are also compared, and the interaction between the ship and the floodwater is analysed. Moreover, the differences between the two wave directions, as well as the possible reasons for such discrepancies, are examined.

2. Mathematical model

2.1 Equation of ship motion

Two right-handed Cartesian coordinate systems are used to describe the motion of the ship in beam seas of regular waves, (Fig. 1). The first one is the *o-xyz* system, in which the origin *o* is fixed on the free surface to describe the fluid motion, the *y*-axis points to the wave direction and the *z*-axis is vertically oriented upward. The other coordinate system is the O-$x_0y_0z_0$ system, which is used to describe the ship motion. The origin O is located at the mass centre of the ship, and the x_0- and y_0-axes point towards the stern and the starboard, respectively. The O- x_0z_0 plane coincides with the mid-longitudinal section. Considering the direction relation of incident wave with the damage opening mainly, the incident wave angle α is defined as the angle between the wave propagation and the y_0-axis, which does not follow the traditional beam wave definition. The incident wave angle α=0° corresponds to the waves that are incident from the opposite side of the damage, whereas α=180° represents those that are incident from the damage side.

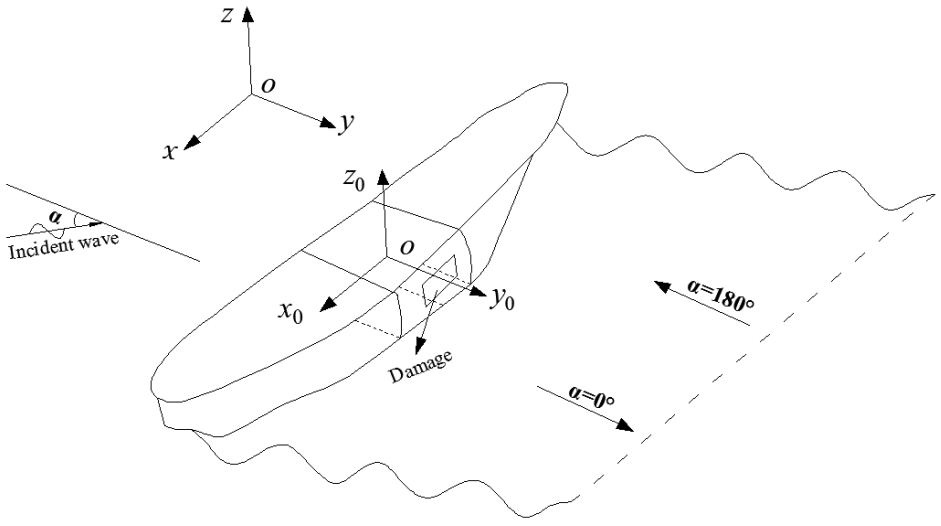

Fig. 1. Coordinate system

The ship motion can be evaluated using the following equations.

$$m\frac{\partial V_i}{\partial t} = f_i$$
$$J_i\frac{\partial \omega_i}{\partial t} + \omega_i \times J_i\omega_i = M_i \tag{1}$$

$$f_i = (f_g + f_{ff})f_r$$
$$f_{ff} = \sum_f (f_f^p + f_f^s) \tag{2}$$
$$f_g = mg$$

$$M_i = \sum_f [r_f \times (f_f^p + f_f^s)] \cdot a \tag{3}$$

where m represents the mass of the ship, V_i represents the velocity of the centre of m, ω_i is angular velocity of mass centre, J_i is the moment of inertia of the ship with respect to the mass centre, f_i and M_i are the resultant force and moment acting on the ship, respectively, f_r is the ramping factor, f_g is the gravity force acting on the body, g is the gravitational vector, f_f^P is the pressure force vector, f_f^s is the shear force vector, x_0 is the longitudinal position of gravity of centre for ship hull, r_f is the position of face f relative to x_0 and a is the vector that defines the axis through point x_0 about which the moment is taken.

2.2 Governing equation

This study discusses incompressible flow involving two different fluids (i.e. water and air). Based on this assumption, the differential forms of the continuity equation and the Reynolds-averaged Navier–Stokes equation are expressed as

$$\frac{\partial u_i}{\partial x_i} = 0 \tag{4}$$

$$\frac{\partial(\rho u_i)}{\partial t} + \frac{\partial(\rho u_i u_j)}{\partial x_i} = \frac{\partial}{\partial x_j}\left[\mu\left(\frac{\partial(u_i)}{\partial x_j} + \frac{\partial(u_j)}{\partial x_i}\right)\right] - \frac{\partial P}{\partial x_i} - \frac{\partial(\rho\overline{u_i' u_j'})}{\partial x_j} + F\,, \tag{5}$$

where $x_i (i = 1, 2, 3)$ represents the coordinate component in the x, y and z direction, u_i denotes the velocity vector components in the x_i direction, ρ is the fluid density, μ is the fluid viscosity, P is the pressure and F is the volume force. The effective density is expressed as $\rho = \varepsilon\rho_1 + (1-\varepsilon)\rho_2$, where ρ_1 and ρ_2 are

the densities of water and air, respectively. The effective viscosity is determined as $\mu = \varepsilon\mu_1 + (1-\varepsilon)\mu_2$, where μ_1 and μ_2 are the viscosities of water and air, respectively, and ε is the fluid volume fraction. ε=1 indicates the water region, ε=0 indicates the air region and 0 < ε<1 represents the interface of water and air. The free surface is captured using the VOF method (Gao, 2010), which is a surface-tracking method that simulates the multiphase flow model by solving the momentum equation and the volume fraction of one or more fluids. The wall function approach, which is applied for the near-wall treatment, is formulated to ensure that reasonable answers will be obtained for the meshes of the intermediate resolution to capture the boundary layer with the acceptable accuracy and time required for the calculation. The turbulence flow model SST k–ω is adopted in this study, and the semi-implicit method for pressure-linked equations algorithm is utilised to determine the pressure and velocity solutions. The dynamic overset mesh strategy is applied to deal with the mesh update between the overset zone and the background and the coupling movement of the rigid boundaries during the flooding process. A commercial CFD solver, STAR CCM+ 2019, is employed to solve the governing equations of the fluid motion. Our preliminary simulation work for damaged ship has validated the feasibility of model and method (Hu, 2019 & 2020). All computations are conducted on a 16-core (Intel Xeon, 2.4 GHz) server computer.

2.3 Wave generation and elimination

In consideration of the restoring moment and obvious influence of the roll, pitch and heave motions on the ship motion, this study adopts the 3-DOF coupling (roll, pitch and heave) to study the motion response under regular beam waves. The waves are introduced from the inlet side as the initial boundary conditions, and the wave elevation and wave field velocity are determined in accordance with Stokes' first wave theory.

$$\eta = A\omega_0 \cos(kx_1 - \omega_0 t) \tag{6}$$

$$u_1 = A\omega_0 \frac{\cosh(kx_3 + kd)}{\sinh(kd)} \sin(kx_1 - \omega_0 t) \tag{7}$$

$$u_3 = A\omega_0 \frac{\sinh(kx_3 + kd)}{\sinh(kd)} \sin(kx_1 - \omega_0 t) \tag{8}$$

where A is the wave amplitude, d is the water depth, k is the wave number, ω_0 represents the wave frequency, x_1 is wave surface location along the wave direction, x_3 is the distance from the water surface and u_1 and u_3 denote the horizontal and vertical velocities, respectively.

To prevent the damping of wave from introducing resistance to vertical motion, the radiation wave must be eliminated by introducing moderate damping before it reaches the entrance boundary. Therefore, the damping and force source terms are added to the momentum equation separately and expressed as follows:

$$
\begin{aligned}
S_1 &= \rho(f_1 + f_2 |u_3|) \frac{e^{\theta} - 1}{e - 1} u_3 \\
\theta &= \left(\frac{x_1 - x_{sd}}{x_{ed} - x_{sd}} \right) \\
S_2 &= \rho f_3 \cos^2\left(\frac{\pi x}{2}\right)(u_i - u_i^*)
\end{aligned}
\tag{9}
$$

where S_1 is the damping term, S_2 is the force source term, x_{sd} is the starting point for wave damping that propagation in the x_1 direction, x_{ed} is the end point for wave damping of the boundary, f_1, f_2 and f_3 are parameters that decided by wave condition, u_i^* is the theoretical solution for the fluid velocity. To reduce the wave reflection effect on the numerical accuracy, the specified wave damping and force value must be at least one wavelength, in the simulation it is two wavelengths.

3. Numerical setup of the DTMB 5415 model

As shown in Fig. 1, two different wave directions, namely, α=180° and α=0°, act on the ship in the beam wave. The ITTC benchmark naval hull form DTMB 5415 is used for roll analysis under damage condition. The scale of the ship model is 1/51, and the parameters are listed in Table 1. Fig. 2 illustrates the hull and the damaged compartment model of DTMB 5415, which has two damaged compartments at the starboard midship with air pipe on the top (Begovic, 2013).

Table 1. Main data of the barge

Parameters	Full scale	Model 51
Length of all (L_{OA}, m)	153.300	3.0
Length of perpendicular (L_{PP}, m)	142.200	2.788
Breath of the waterline (B_{WL}, m)	19.074	0.374
Depth (D, m)	12.470	0.244
Draft (T, m)	6.150	0.120
Displacement (Δ , m^3)	8424	0.0635
Metacentric height (GM, m)	1.938	0038
Centre of gravity above the baseline (KG, m)	7.555	0.148
Roll radius of gyration (k_{xx}-WATER, m)	6.932	0.136
Pitch and yaw radius of gyration (k_{yy}-AIR, m)	0.25*L*	0.25*L*
Area of the damaged opening (A_0, m^2)	58.148	0.022

Volume of floodwater (∇_w, m^3)	2639	0.0199

3.1 Computational domain and boundary conditions of the beam wave

The computational domain is divided into the background and overset regions. The dimensions are set in accordance with the ITTC procedures and guidelines (ITTC, 2011), as shown in Fig. 3. The locations of the port and starboard side are at 4λ, the length is $3L$, the water depth is 2.15 m and the height above the water surface is 2 m. The elimination zone starts at 2λ away from the inlet and outlet boundaries. All boundary conditions are defined in the numerical setup. The no-slip wall boundary condition is imposed on the top and bottom parts, and the front and back sides are symmetric. The starboard side and port are set as the velocity inlet and pressure outlet, respectively, when α =180°; the functions are reversed when α =0°. In the left, right, front and back boundaries of the domain, the water level is set to the initial water height, and a regular beam wave is spread from the boundaries to the computational domain. The moment of inertia of the model can be calculated from the weight distribution manual.

Figs. 4 and 5 depict the mesh arrangement in the computational region and the mesh near the ship, respectively. The wave generation mesh should guarantee that the wave height and length direction are consistent with the ITTC criteria (ITTC, 2014). To avoid large computational cost, a suitable mesh is generated by adjusting the wave height and the length direction. This mesh is gradually coarsened away from the ship and the damage opening (Table 2). H denotes the wave height and λ is the wavelength. The mesh in the overset region and free surface is condensed at 0.0125λ and $0.1H$ along the y (i.e. wave propagation direction) and z directions, respectively. The rate of increase in the wave generation and elimination zones is 1.05, whereas that in other regions is 1.15. Trimmed mesh elements are generated for the whole computational domain, similar mesh setting in still water is verified effective based on our previous simulation work for damaged ship (Hu, 2019 & 2020), computational mesh is designed to solve the hull geometry, boundary layer, flooding dynamics and wave field with acceptable simulation time, so the mesh setting discussion is omitted here, also the dependency analysis of time step is carried out to reach a balance between simulation time and accuracy.

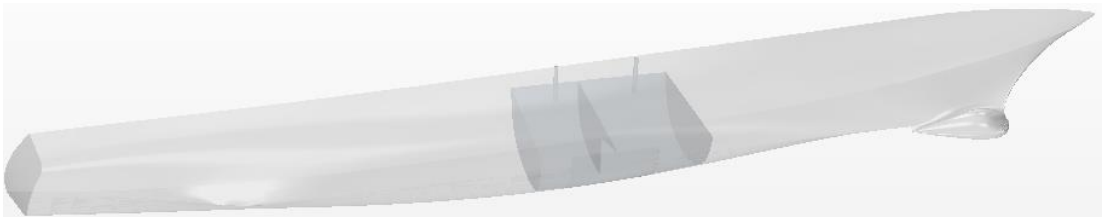

Fig. 2. Geometry of the ship and the damaged compartment

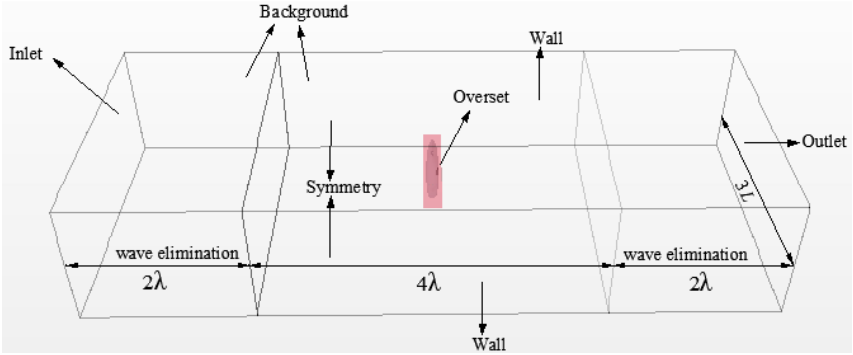

Fig. 3. Computational domain

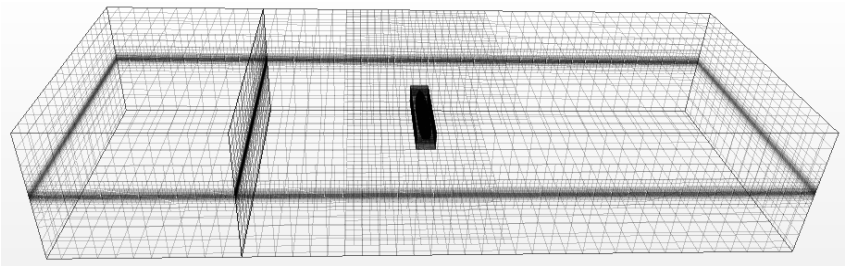

Fig. 4. Sketch of the mesh arrangement in the computational region

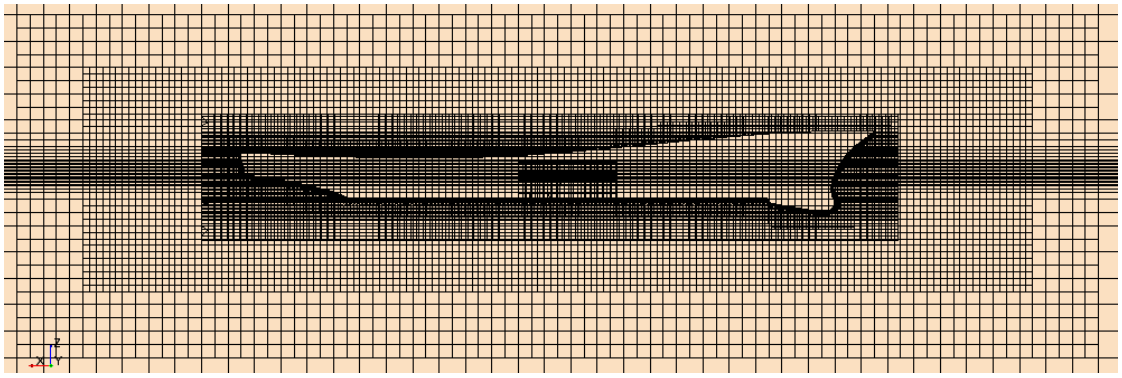

Fig. 5. Sketch of the mesh arrangement near the ship

Table 2. Dimensions of the mesh used in wave generation

Region	Mesh dimension	
	y	z
Overset	0.0125λ	$0.1H$
Wave elimination	$0.0125\lambda \times 1.05$	$0.1H \times 1.05$
Wave generation	$0.0125\lambda \times 1.05$	$0.1H \times 1.05$
Free surface	0.0125λ	$0.1H$
Other region	$0.0125\lambda \times 1.15$	$0.1H \times 1.15$

3.2 Wave generation and independence analysis

The time step test is performed to investigate the numerical accuracy of the wave generation. A wavelength λ of 2.8 m is selected as the target example because it is within the harmonic region. The time step is set to 1/400, 1/600 and 1/800 wave period (T_W), and the simulation runs for 60 s (approximately 40 T_W). The simulations for the three T_W values require 2.5, 3.5 and 4.5 CPU hours for a one-second calculation, respectively. The simulated wave elevation is compared with the theoretical value. The time-domain wave elevation from the inflow boundary 6λ is shown in Fig. 6. The simulation accuracy improves with the decrease in the time step. The comparisons imply that no obvious difference exists between 1/600 and 1/800 T_W, which are in accordance with the theoretical value. Conversely, the difference for 1/400 T_W increases due to the decreased time step. Fig. 7 shows that no obvious difference is observed amongst the three time steps in the wave generation region. In the figure, y represents the incident wave propagation direction. When the waves arrive at the elimination area, substantial differences are observed in simulation with the theoretical wave. This phenomenon indicates that the waves are eliminated in the outlet boundary.

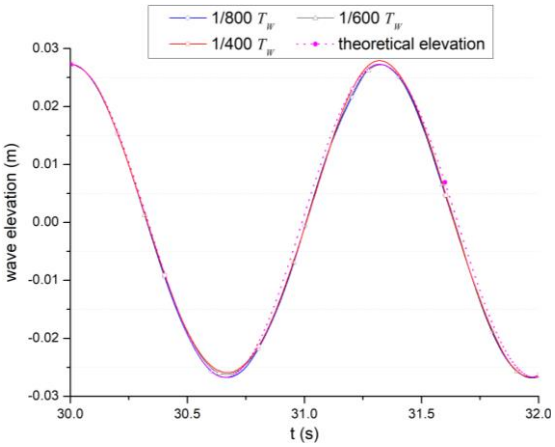

Fig. 6. Wave elevation from the inflow boundary (6λ)

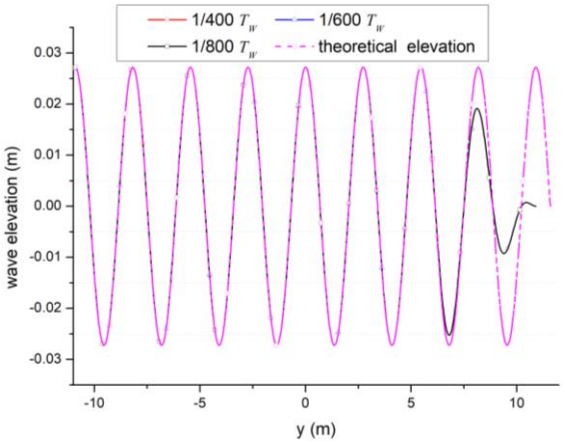

Fig. 7. Wave elevation in the computational domain

The wave generation test is conducted by simulating the wave condition at different wavelengths. Fig. 8 displays the free surface coloured with the elevation for a regular beam wave at λ=2.8 m with a time step of $T_W/600$. Considering a draft of 0.12 m as reference, the position in the *z* direction implies that the wave elevation in the numerical tank might be in consistent with the theoretical value for the two incident wave directions. Therefore, $T_W/600$ is adopted as the time step value to ensure satisfactory accuracy and acceptable cost.

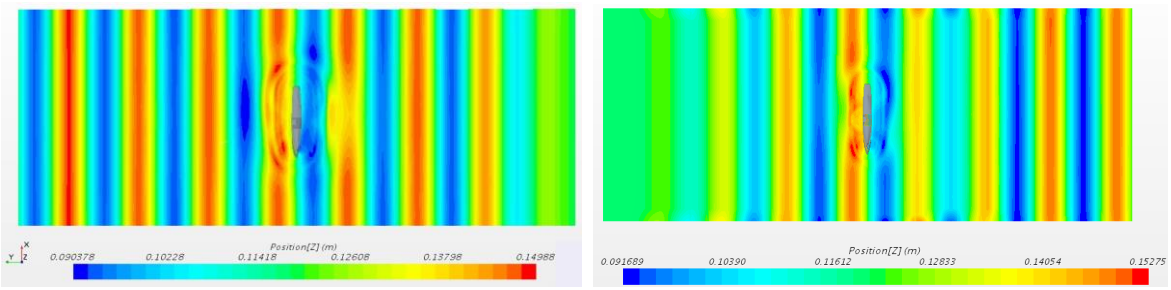

Fig. 8. Simulated regular beam waves (left: α =180°; right: α =0°)

4. Numerical results

4.1 RAO analysis

On the basis of the independence analysis, the damaged ship motion in regular beam wave with different wavelengths is analysed to investigate the ability of the adopted method to solve such motions. The 3-DOF coupling of roll, pitch and heave motions are considered in the calculation. The wave steepness is 0.02, and the time step is $T_W / 600$. The wave frequency ω changes from 2.812 rad/s to 5.606 rad/s, and the corresponding λ ranges from 1.960 m to 7.791 m. The wave parameters are summarised in Table 3. At the initial simulation stage, the water surface in the compartment is the same as the static waterline. The simulation, which requires 3.5 CPU hours for a one-second simulation run, continues until the ship motion stabilises (approximately 20–30 T_W cycles).

Table 3. Wave parameters of the model scale for the RAO analysis

Number	Wave frequency ω (rad/s)	Wavelength λ (m)	Wave height H (m)	Roll response (°)		Error	
				Experiment	Simulation	Absolute(°)	Relative(%)
1	2.812	7.791	0.156	6.704	6.843	0.139	2.073
2	3.234	5.890	0.118	8.283	8.440	0.157	1.895
3	3.419	5.270	0.105	11.186	11.427	0.241	2.154
4	3.717	4.459	0.089	13.637	13.865	0.228	1.672
5	4.086	3.690	0.074	15.675	16.295	0.62	3.955
6	4.269	3.380	0.068	16.478	16.620	0.142	0.862
7	4.517	3.023	0.060	15.484	15.580	0.096	0.620
8	4.691	2.792	0.056	6.417	7.250	0.833	12.981
9	5.004	2.460	0.049	2.979	3.909	0.93	31.219
10	5.606	1.960	0.039	1.99	2.501	0.511	25.678

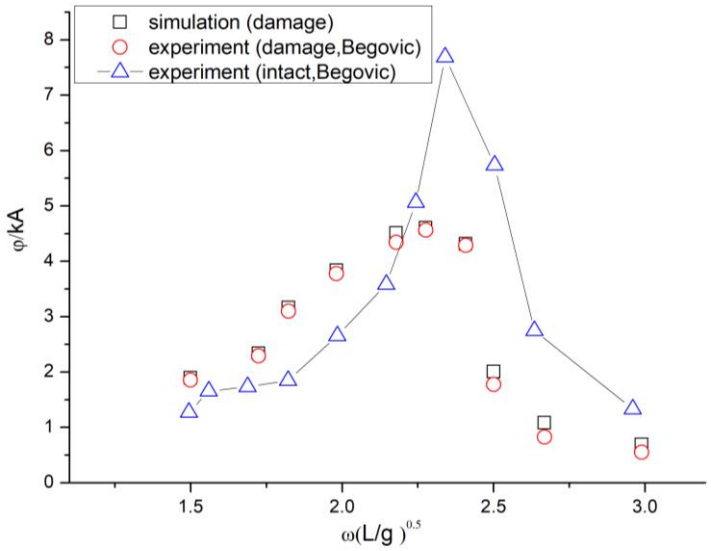

Fig. 9. Comparison of the roll RAOs obtained through simulation and experiment

In accordance with the wave parameters presented in Table 3, Fig. 9 shows the computed and measured roll RAOs of the DTMB 5415 model under damaged conditions at α =180°. The experimental RAOs of the intact ship are also listed for comparison and analysis. The roll amplitudes are non-dimensionalised by kA (wave number × wave amplitude). To present a uniform non-dimensional demonstration in the plots between the motion frequency and amplitude, the frequency is also non-dimensionalised by multiplying $(L/g)^{0.5}$ for comparison, where L is the length of the ship model. Compared with the roll motion of the intact ship, the peak response of the damaged ship is considerably reduced due to the energy dissipated by the flow entering or exiting the damaged compartments. The amplitude of the motion calculated via numerical simulation is slightly higher than that obtained through experiment. With regard to the reduction of the computational cost, the computational domain adopted and mesh arrangement outside the ship might not ensure the exact representation of the external wave pattern. This limitation can affect the behaviour of the flooding water inside the compartment. The errors between the numerical and experimental results are included in Table 3. The maximum errors of the roll amplitude amongst these results are less than 1°. Although the peak magnitude is slightly overpredicted in the simulation of the incident wave frequencies outside the harmonic zone, the trend of the computed RAOs is consistent with the experimental data for the harmonic frequencies. In harmonic zone the roll amplitudes are larger than the non-harmonic frequencies, which vary from 6° to 16°, but the relative errors are small due to nearly the same absolute errors, the errors between the numerical simulation and experiment vary with the wave parameters. The possible reason could be the roll damping, wave-induced force and roll moment error lying in numerical calculation, in which the viscosity plays an important role and has great effect on the rolling motion, this could exert error with the experiment measurement. Apart from this numerical calculation

error, the wave elevations that generated by RANS solver might not constantly be the same with the wave maker in physical tests.

Figs. 10 and 11 present the roll motion of the damaged ship in the time domain at two different frequencies with α =180°. The experimental result shows that the roll natural frequency ω_{φ} of the damaged ship is 4.135 rad/s (Begovic, 2015). The frequencies within the harmonic zone (4.517 rad/s) and near the ship's roll frequency (4.269 rad/s) are selected as references. FFT is used to determine the natural frequency of the ship's roll motion. When the incident wave frequency changes from 4.517 rad/s to 4.269 rad/s, the frequency of the peak response shifts from 4.6 rad/s to 4.312 rad/s. As shown in Fig. 11, the latter is close to the ship's roll natural frequency, where the maximum roll response easily occurs. This finding is consistent with the experimental data.

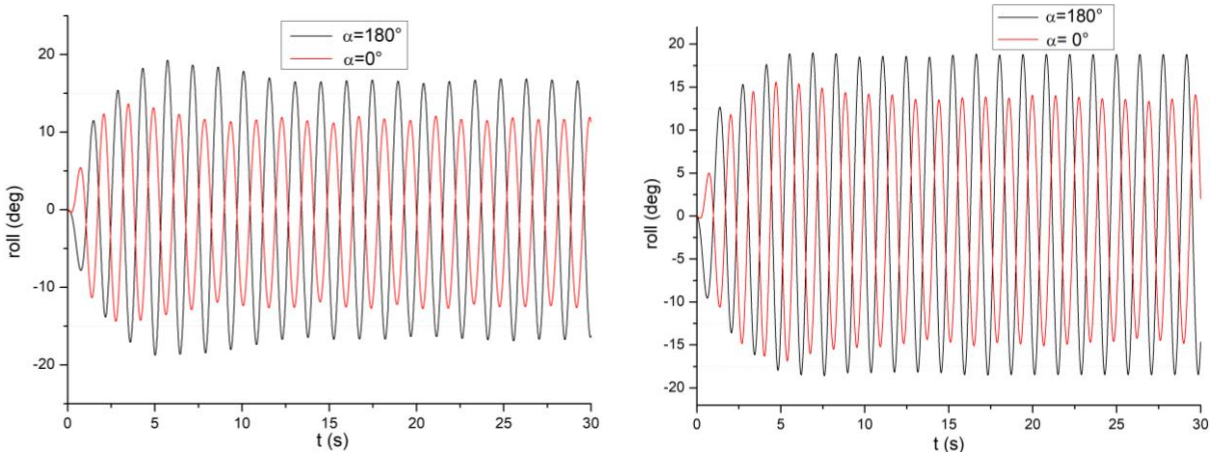

Fig. 10. Comparison of the ship's roll motion in the time domain at different frequencies (left: ω =4.517 rad/s; right: ω =4.269 rad/s)

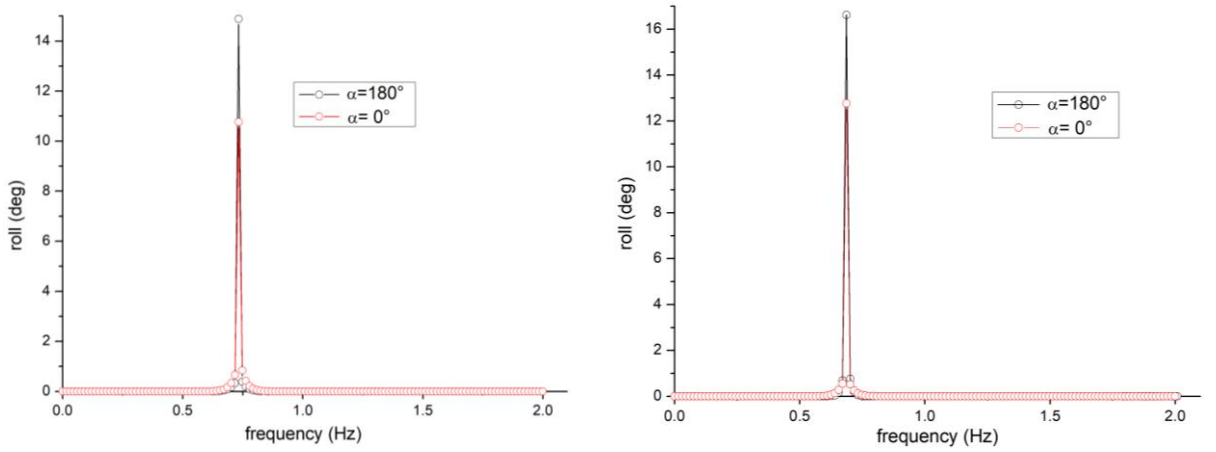

Fig. 11. Comparison of the FFT results of the roll motions at different frequencies (left: ω =4.517 rad/s; right: ω =4.269 rad/s)

To investigate the roll response difference amongst different wave directions, the damaged ship motion and the FFT at α =0° are analysed and compared with the corresponding values at α =180°. The computational

domain, wave parameters, boundary conditions and time step introduced in Section 3 are applied. The comparison of the two harmonic frequencies shows that the roll response at α =180° is greater than that at α =0°, and the frequency of the peak response demonstrates good agreement within the two wave directions.

The simulated RAOs at α =0° (Fig. 12) are compared with those at α =180° for the same frequency range.

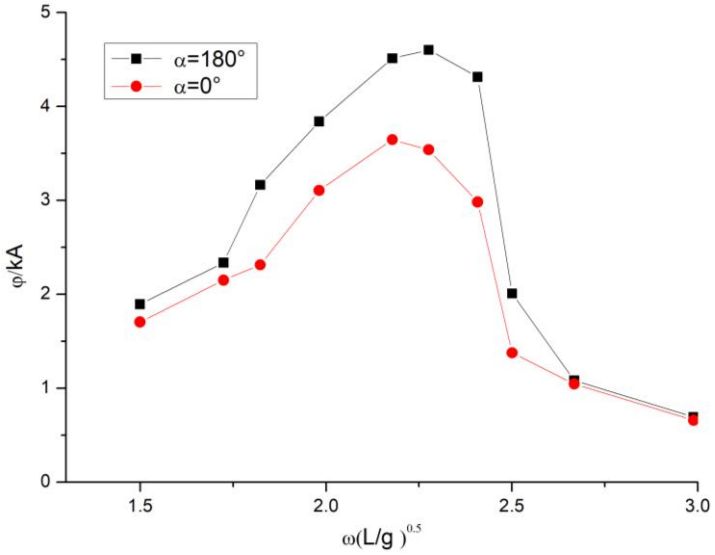

Fig. 12. Comparison of the roll RAOs at α =180° and α =0°

Fig. 12 indicates that the roll amplitude of α =0° is smaller than that of α =180°, especially in the harmonic zone. The difference of the roll peaks obtained by these two beam wave directions are roughly 4.81°. The comparison results show that the harmonic zone can enlarge the difference between the two wave directions. Taking a harmonic wave frequency of 4.517 rad/s as example, the time-domain roll responses of intact and damaged ships at α =0° and α =180° are compared (Fig. 13). The roll response of the intact ship is the largest, whereas the damaged ship of α =0° is the smallest. After the ship motion stabilises, the roll differences between three conditions are 5.1°, 11.9° and 17°. According to the multi-DOF roll motion equation, the roll amplitude is closely related to the roll moment. To analyse the possible reason for the observed discrepancies, the wave excitation and flooding water heeling moments and their coupling action in each wave direction are analysed (Figs. 14 and 15). The flooding water heeling moment counteracts the wave excitation moment. Therefore, the roll moment of the damaged ship greatly decreases compared with that of the intact ship, and the effect of wave excitation is partly weakened by the water flooding. The decrease in the roll moment of the damaged ship at α =0° is greater than that at α =180°, so the roll amplitude at the former is smaller than that at the latter. This inference can be verified by the time history of the floodwater volume in Fig. 16. The figure suggests that

because the flooding water heeling moment is greater at α=0° than that at α=180°, it can generate many interference and demonstrate violent motion characteristics. As a result, the total roll moment after coupling with the wave excitation moment is small.

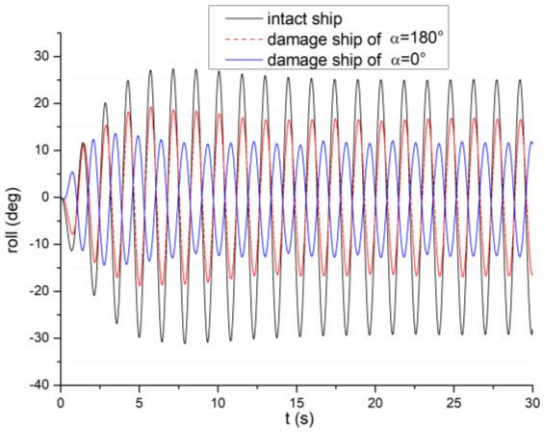

Fig. 13. Comparison of the roll responses at different wave conditions

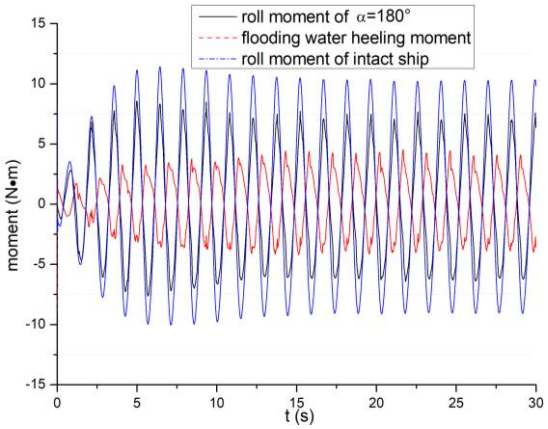

Fig. 14. Moment at α=180°

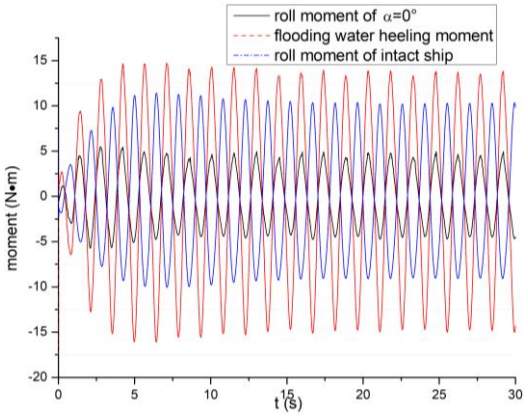

Fig. 15. Moment at α=0°

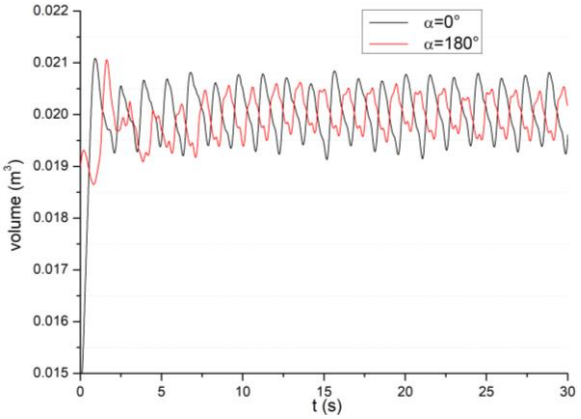

Fig. 16. Comparison of the time history of flooding water volumes

4.2 Ship motion analysis

To demonstrate the behaviours of the damaged ship motion in the two beam wave directions, the 3-DOF model that considers the roll, pitch and heave motions is used to analyse the ship motion in waves. To investigate the damaged ship motion, the compartment is emptied, and the water started to flood into the damaged opening at the initial simulation stage. The time-domain motion responses at α=180° and α=0° under regular beam waves with frequencies of ω=2.812, 4.269, 5.606 rad/s are presented in Figs. 17–19, respectively. The snapshots of the roll motions of the ship and floodwater at a frequency of 4.269 rad/s at α=180° and α=0° are shown in Figs. 20 and 21, respectively.

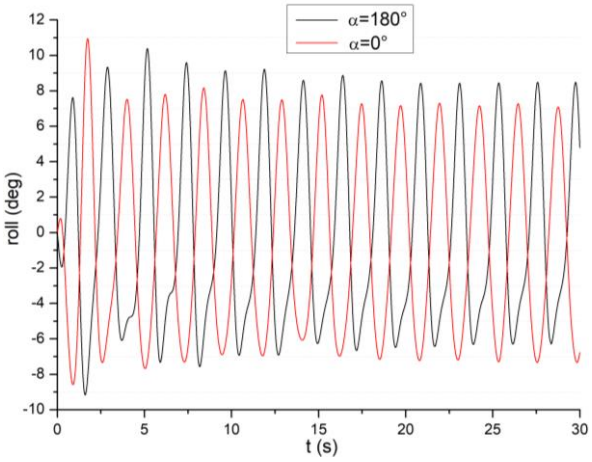

(a) Roll motion

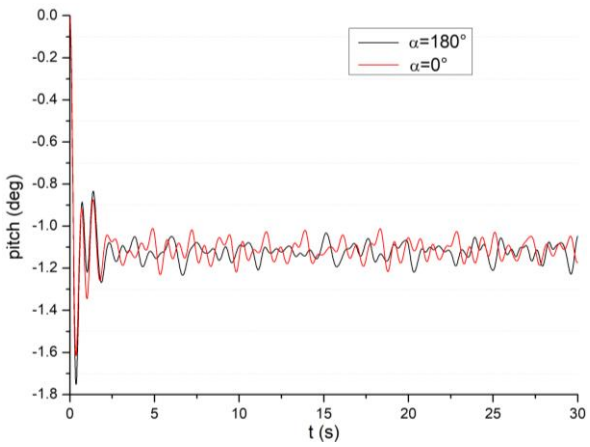

(b) Pitch motion

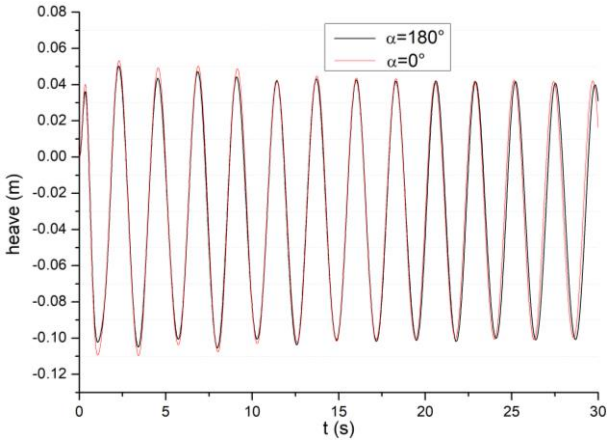

(c) Heave motion

Fig. 17. Motion response comparison (ω =2.812 rad/s)

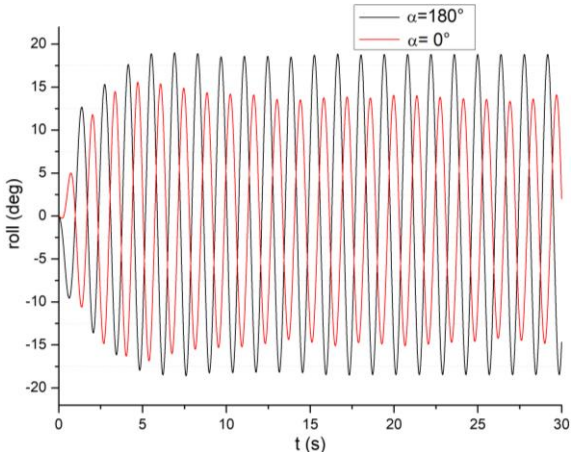

(a) Roll motion

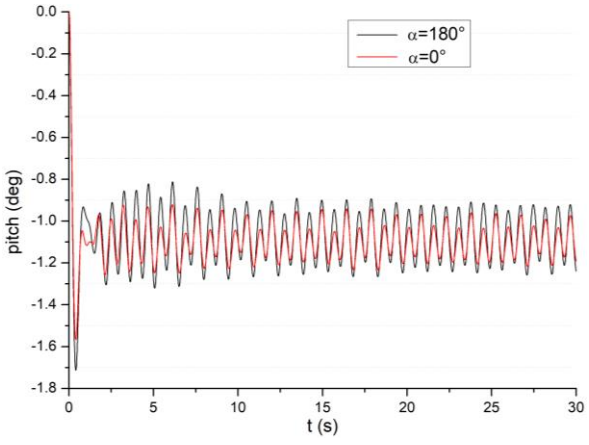

(b) Pitch motion

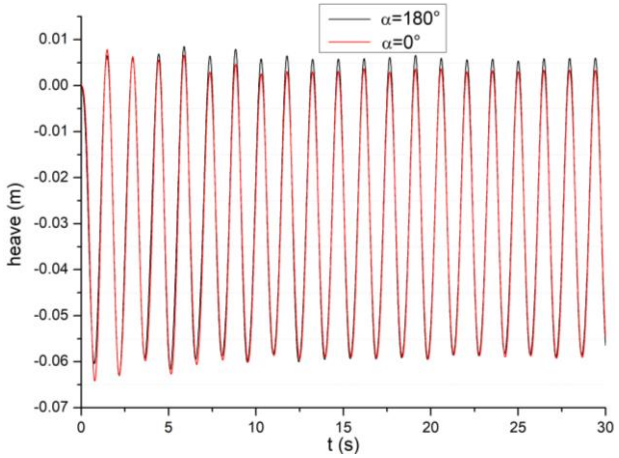

(c) Heave motion

Fig. 18. Motion response comparison (ω =4.269 rad/s)

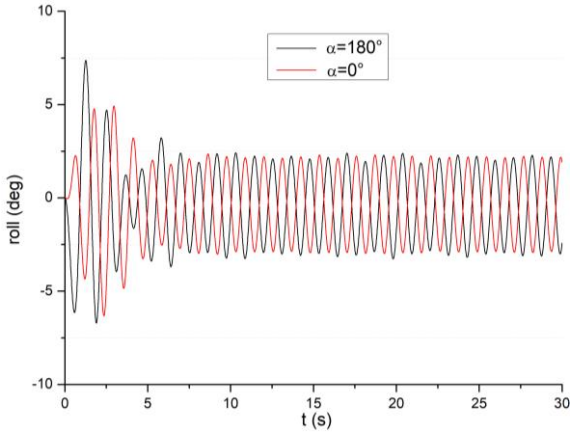

(a) Roll motion

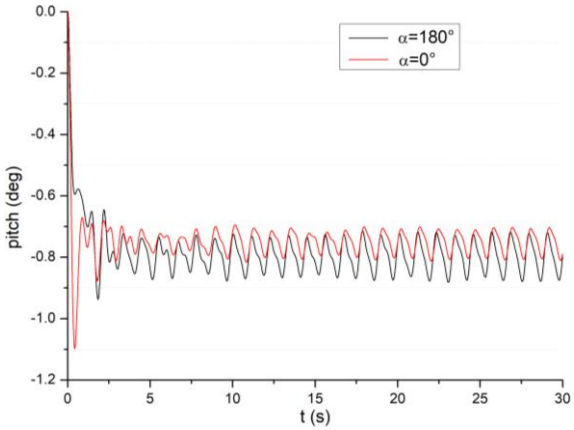

(b) Pitch motion

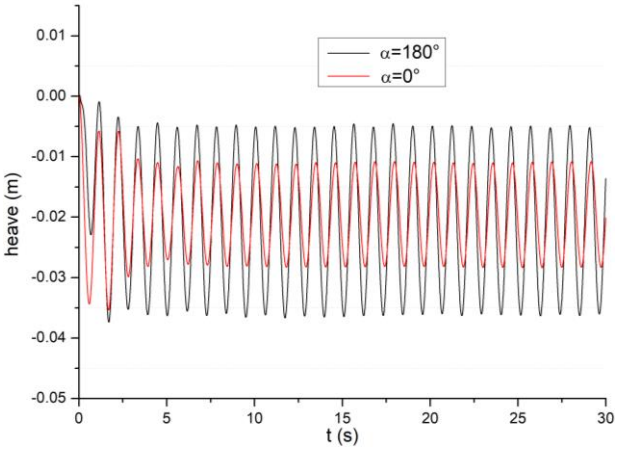

(c) Heave motion

Fig. 19. Motion response comparison (ω =5.606 rad/s)

The wavelength at a wave frequency of 2.812 rad/s is approximately two times the ship length. The wave height increases when the wavelength increases with a certain wave slope. Given that the heave motion is sensitive to the incident wave amplitude, this motion has the greatest amplitude amongst the three wave frequencies. However, the roll is small because the wave frequency is far from the ship's natural frequency, and the shift of the 3-DOF model demonstrates the same tendency between the two wave directions. A wave frequency of 4.269 rad/s is close to the damaged ship's roll natural frequency. Comparing this value with the other two high and low frequencies, its roll motion amplitude is the largest in the 3-DOF model. The ship motion stabilises at roughly 13 s for the two wave conditions. The roll amplitude at α =180° is 16.62°, whereas that at α =0° is 12.77°. The pitch amplitude is small, which is 0.272° at α =180° and 0.179° at α =0°. Similarly, the heave amplitude between the two wave directions is small. The wavelength at a wave frequency of 5.606 rad/s is more than half the ship length, which is equal to the ship cruises in a short wavelength. Therefore, the roll amplitude is small, which is 2.501° at α =180° and 2.379° at α =0°，the difference between the two wave directions are extremely small, and the pitch and heave amplitudes at α =180° are greater than those at α =0°. The comparison of the three wave frequencies indicates that the roll amplitude is the largest when the wave period is close to the ship period because of the harmonic response. In addition, the roll amplitude at α =180° is greater than that at α =0°, that is, the latter is safer than the former. This inference can serve as a useful guide in case of flooding emergency. To effectively reduce the roll motion of the damaged ship, the wave direction can be adjusted from α =180° to α =0°, especially in the harmonic wave zone.

Figs. 20 and 21 show the transverse view of the floodwater motion in the time domain at a wave frequency of 4.269 rad/s at α =0° and α =180°. The flooding water starts to enter the ship at the initial stage. When the water almost reaches the tank top, a large quantity of water floods the compartment through the damage opening. With the increase in the amount of flooding water, the water motion in the compartment becomes violent, and sloshing is initiated. As a result, the free surface is subject to a series of rolling until it finally reaches the quasi-static stage. The floodwater motion at α =0° is more turbulent than that at α =180°, and thus can couple with the ship motion to a great degree and prevent the ship from heeling with a large angle. This finding is consistent with the results shown in Fig. 13.

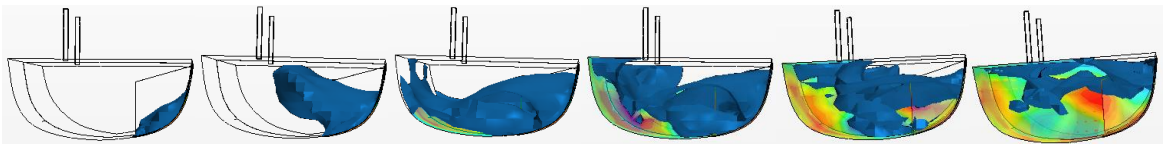

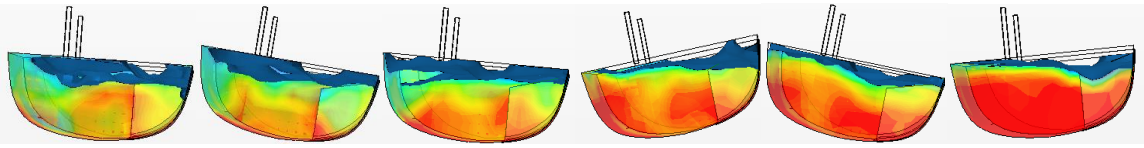

Fig. 20. Snapshots of roll motion at α=0° (ω=4.269 rad/s)

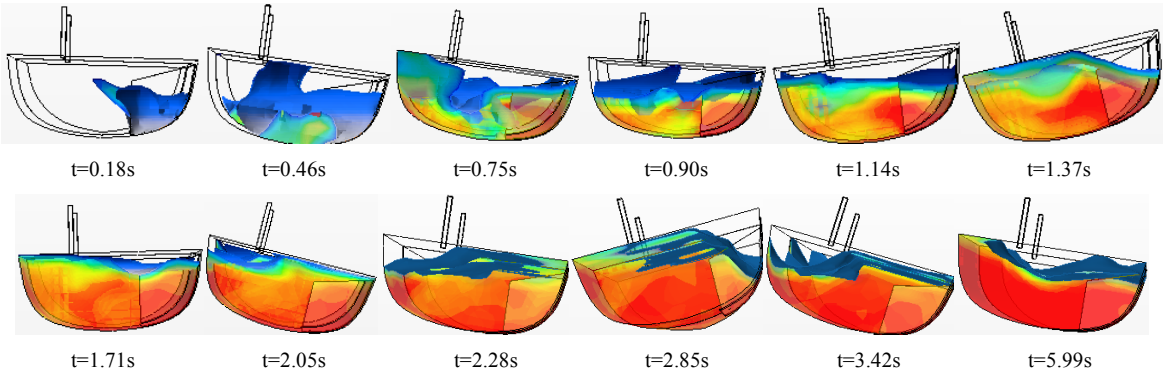

Fig. 21. Snapshots of roll motion at α=180° (ω=4.269 rad/s)

5. Conclusion

This study presents the motion behaviour of a damaged ship (DTMB 5415) in waves that come from two different beam waves directions, namely α=180° and α=0°. The adopted method is to solve the RANS equations by using the VOF free-surface technique and the dynamic mesh strategy to tackle the interaction between the ship and the wave. On the basis of the motion analysis at α=180°, α=0° is used to conduct the ship motion response. The comparison of the RAOs at α=180° obtained through numerical simulation and experiment indicates that the method involving the wave generation, time step and mesh arrangement can effectively deal with ship flooding in regular beam waves. On the basis of this verification, the RAOs and ship motion at α=0° is compared with those at α=180°.

According to the numerical analysis results, the main findings are as follows: Firstly, the roll motion amplitude of the damaged ship is smaller than that of the intact ship. Given the coupling motion of the wave excitation and the heeling moment produced by flooding water, various differences are observed in the value of the roll amplitude, and the flooding water effect turns into the damping of ship rolling. Secondly, the roll response of the damaged ship at α=0° is smaller than that at α=180° for the same reason. The roll amplitude varies with the wave parameter, which is the largest in harmonic region and closely related with fluid viscosity consideration, so it is the main reason that leads to calculation error. The roll peak difference between α=0° and α=180° lies in the harmonic zone and reaches a value of 4.81°. This difference can therefore decrease the capsizing risk by adjusting the ship and wave locations and serve as a useful guide in case of flooding emergency.

Thirdly, the flooding water heeling moment could work as the anti-roll moment to prevent the ship rolling to a larger degree, which could be helpful for the ship roll motion control. Finally, the transverse view comparison of the floodwater motion in the two wave directions indicates that the time-domain roll motion at α =0° is more turbulent than that at α =180°. Several phenomena, such as rolling, climbing and sloshing, are captured by the free surface. However, the above-mentioned analysis is based only on simulations under regular beam waves. The seakeeping performance under irregular waves should be further analysed in the future.

Acknowledgments

This study was supported financially by the National Natural Science Foundation of China (Grant Nos. 51509124, 51979131 and 51681340360). The authors extend their sincere gratitude to the abovementioned organizations. We are also grateful for the suggestions, important references, and summaries offered by the anonymous reviewers who improve the quality of this work and this paper.

References

[1]. Begovic, E., Mortola, G., Incecik, A., Day, A. H., 2013. Experimental assessment of intact and damaged ship motions in head, beam and quartering seas. Ocean Engineering, 72, 209-226.

[2]. Bu, S., Gu, M.. 2019. Study on the damaged ship motion coupled with damaged flow based on the unified viscous/potential prediction model, Proceedings of the 17th International Ship Stability Workshop, 209-220, Helsinki, Finland.

[3]. Chan, H., Atlar, M., Incecik, A., 2002. Large-amplitude motion responses of a Ro-Ro ship to regular oblique waves in intact and damaged conditions. Journal of Marine Science and Technology, 7(2), 91-99.

[4]. de Kat, J. O., Paulling, J. R., 2001. Prediction of extreme motions and capsizing of ships and offshore marine vehicles. Proceedings of the 20th International Conference on Offshore Mechanics and Arctic Engineering, 1-12, Rio de Janeiro, Brazil.

[5]. Gao, Q., Vassalos, D., 2011. Numerical study of the roll decay of intact and damaged ships. Proceedings of the 12th International Ship Stability Workshop, 277-282, Washington, USA.

[6]. Gao, Z., Gao, Q., Vassalos, D., 2013. Numerical study of damaged ship flooding in beam seas. Ocean Engineering, 61, 77–87.

[7]. Gao, Z., Wang, Y., Su, Y. 2020. On damaged ship motion and capsizing in beam waves due to sudden water ingress using the RANS method. Applied Ocean Research, 95, 102047.

[8]. Gu, Y.. 2019. Experimental and numerical investigation on wave-induced loads acting on intact and damaged naval combatant vessel. Ph.D. Thesis, Universities of Strathclyde.

[9]. Hu, L., Qi, H., Li, Y., Li, W., Chen, S., 2019. The CFD Method-based Research on Damaged Ship's Flooding Process in time-domain, Polish Maritime Research, 26(1), 72-81.

[10]. HU L., WU H., GONG Q., et al., 2020. Time-Domain Flooding Simulation of a Damaged Warship, Marine Technology Society Journal, 54(2): 1-10.

[11]. Ikeda, Y., Himeno, Y., Tanaka, N., 1978. Components of roll damping of ship at forward speed. Journal of the Japan Society of Naval Architects and Ocean Engineers, 143, 1-14.

[12]. ITTC Recommended Procedures and Guidelines, 2014. Practical Guidelines for Ship CFD Applications. 7.5-03-02-03.

[13]. ITTC Recommended Procedures and Guidelines, 2011. Practical Guidelines for Ship CFD Applications. 7.5-03-02-03.

[14]. Lee, D., Hong, S.Y., Lee, G.J., 2007. Theoretical and experimental study on dynamic behavior of a damaged ship in waves, Ocean Engineering, 34, 21–31.

[15]. Manderbacka, T. L., Matusiak, J. E., 2011. Ship motions caused by time-varying extra mass on board. Proceedings of the 12th International Ship Stability Workshop, 263-269, Washington, USA.

[16]. Ruponen, P.. 2007. Progressive flooding of a damaged passenger ship. Ph.D. Thesis, Helsinki University of Technology.

[17]. Ruponen, P., Lindrotha, D., Routic, A., Aartovaarac, M., 2019. Simulation-based analysis method for damage survivability of passenger ships. Ship Technology Research, 66(3), 182–194.

[18]. Ruth, E., Olufsen, O., Rognebakke, O.. 2019. CFD in damage stability, Proceedings of the 17th International Ship Stability Workshop, 259-263, Helsinki, Finland.

[19]. Sadat-Hosseini,H., Kim, D.H., Carrica, P.M., Rhee, S.H., Stern, F., 2016. URANS simulations for a flooded ship in calm water and regular beam waves, Ocean Engineering, 120, 318–330.

[20]. Spanos, D., Papanikolaou, A., 2001. On the stability of fishing vessels with trapped water on deck. Ship Technology Research, 48(3), 124-133.

[21]. Strasser, C.. 2010. Simulation of progressive flooding of damaged ship by CFD. Ph.D. Thesis, Universities of Glasgow and Strathclyde.

[22]. Turan, O., Vassalos, D., 1993. Dynamic stability assessment of damaged passenger ships. Transactions of the Royal Institution of Naval Architects, 135, 79-104.

[23]. Wang, Q., Chen, X., Liu, L., Wang, X., 2019. Numerical Simulation of Damaged Ship's Motion in Beam Waves. Proceedings of the ASME 38th International Conference on Ocean, Offshore and Arctic Engineering, 1-8, Glasgow, Scotland.